One-pot mechanochemically-assisted synthesis of Cu$_2$O/GO nanocomposites with enhanced photocatalytic activity

LONGFENG LI[a,b], PEIPEI XIAO[a], MAOLIN ZHANG[a,b*], MINGZHU LIU[a*]

[a]*School of Chemistry and Materials Science，Huaibei Normal University，Huaibei 235000, PR China*
[b]*Information College, Huaibei Normal University，Huaibei 235000, PR China*

Cu$_2$O/GO nanocomposites are successfully synthesized by a facile room-temperature ball-milling assisted solid-state reaction and subsequent heat treatment, using Cu(OH)$_2$CO$_3$, H$_2$C$_2$O$_4$·2H$_2$O and graphene oxide (GO) as the raw materials. The intermediate product Cu$_2$(OH)$_{2n}$(CO$_3$)$_{1-n}$C$_2$O$_4$/GO (n=0~1) is firstly formed by milling Cu(OH)$_2$CO$_3$, H$_2$C$_2$O$_4$·2H$_2$O and GO powders at room temperature, then this intermediate product is further heated under the protection of nitrogen atmosphere at 350 ℃ to form Cu$_2$O/GO nanocomposites. This makes it a new promising approach for Cu$_2$O/GO nanocomposites, which is simple and environmentally friendly. The morphology and phase structure of the synthesized products are characterized by field emission scanning electron microscopy (FE-SEM), transmission electron microscopy (TEM) and X-ray diffraction (XRD). The photocatalytic performances of the obtained products are evaluated by analyzing the degradation of methyl orange (MO) solution under visible-light irradiation. The Cu$_2$O/GO nanocomposites show higher photocatalytic activities than pure Cu$_2$O attributing to the synergistic effect of Cu$_2$O and GO, and the 50Cu$_2$O/GO nanocomposite exhibits a highest efficiency for photocatalytic degradation of MO.

1. Introduction

Semiconductor photocatalysis has attracted increasing attention as a potential technology for the pollutants degradation during the past decades. To date, although various active oxide semiconductor photocatalysts have been rapidly developed, there are still some problems remaining to be solved. On the one hand, the wide-band-gap semiconductor oxides are only sensitive to UV light, which accounts for less than 5% of the total solar energy that reaches the Earth. Therefore, great efforts have been made in exploring new visible-light-responsive photocatalysts in order to utilize a larger portion of solar energy. At present, cuprous oxide (Cu$_2$O), a p-type semiconductor with a narrow-band-gap of 2.0 eV, has been proved to be the most promising candidate for visible-light-driven photocatalytic decontamination [1-6]. On the other hand, it is well known that graphene is an atomic sheet of sp^2-bonded carbon atoms that are arranged into a honeycomb structure. Apart from its unique electronic properties, the 2D planar structure material has several other excellent attributes, such as the large theoretical specific surface area and the high transparency due to its one-atom thickness. Therefore, the graphene-based Cu$_2$O semiconductor composite is promising to exhibit high photocatalytic performance, attributing to the synergistic effect of Cu$_2$O and graphene,

which features: (i) a broader range of light absorption; (ii) faster interfacial charge separation and transfer; and (iii) lower recombination possibility of photogenerated electrons and holes. And previous studies have also shown that the graphene-based Cu$_2$O semiconductor composite exhibit high photocatalytic efficiency [7–20].

In this study, we present a low-cost, fast, facile, green strategy, namely a one-pot mechanochemically assisted approach involving ball-milling assisted solid-state reaction and subsequent heat treatment has been developed for the controlled synthesis of Cu$_2$O/GO nanocomposites. During the facile procedure, no solvent, additive agent, or other complex reaction conditions are required. At the same time, the photocatalytic activities of the as-synthesized Cu$_2$O/GO nanocomposites are tested by the degradation of methyl orange (MO) solution under visible-light irradiation.

2. Experimental

2.1 Materials and apparatus

Cu$_2$(OH)$_2$CO$_3$ and H$_2$C$_2$O$_4$·2H$_2$O used in the study were of analytical grade quality, and graphene oxide (GO) nanoplatelets (thickness: 0.55-1.2 nm) were purchased

from Beijing DK nano technology Co., LTD and used as received. A powder diffractometer (Bruker D8 Advance, Germany) with Cu Kα radiation (λ= 0.15418 nm), the accelerating voltage of 40 kV and the emission current of 40 mA was used to determine the crystal phase composition and the crystallite size of the synthesized samples. A scanning electron microscope (Hitachi S-4800, Japan) and a transmission electron microscope (HT7700, Japan) were employed to observe the shape and size of the synthesized samples.

2.2 Synthesis procedure

In a typical synthesis process, the initial reactants $Cu_2(OH)_2CO_3$, $H_2C_2O_4 \cdot 2H_2O$ and GO were firstly mixed together in a certain amount ratio. Then, the mixture was allowed to have a ball milling reaction using the planetary ball mill (QM-3SP04, China) with zirconium oxide tanks at the rotation speed of 480 rpm for a certain time at room temperature. Finally, the obtained intermediate products were calcined at a certain temperature under the protection of nitrogen for 1 h to get Cu_2O/GO nanocomposites. Referring to our previous study [5], the ball milling time was set for 60 min and the calcination temperature was fixed at 350 °C.

2.3 Photocatalytic activity test

The photocatalytic degradation experiments were carried out in a photochemical reactor using a 500 W Xe lamp with a 420 nm UV cutoff filter, and the photocatalytic performance of the prepared Cu_2O/GO was evaluated by the photodegradation of MO. The reaction temperature was kept at room temperature by cooling water to prevent any thermal catalytic effect. The reaction suspension was prepared by adding 0.25 g of the Cu_2O/GO powder into 100 ml MO aqueous solutions with the concentration of 20 mg/L. Prior to irradiation, the suspension was magnetically stirred in a dark to reach the adsorption/desorption equilibrium between photocatalyst and MO. The degradation of MO was evaluated by centrifuging the retrieved samples and recording the intensity of absorption peak of MO (464 nm) relative to its initial intensity (c/c_0) using a spectrophotometer.

3. Results and discussion

3.1 Synthetic principle of Cu_2O/GO composites

The preparation of Cu_2O/GO composites is a two-stage process. At the first stage, the mixed reactants (the molar ratio of $Cu_2(OH)_2CO_3$ to $H_2C_2O_4 \cdot 2H_2O$ is 1:1; the mass ratio of $Cu_2(OH)_2CO_3$ to GO is m:1, m = 5~70) are ball-milled for a period of time, which can lead to the solid state reaction of $H_2C_2O_4 \cdot 2H_2O$ and $Cu_2(OH)_2CO_3$ and form the intermediate product of

$Cu_2(OH)_{2n}(CO_3)_{1-n}C_2O_4$/GO (n=0~1), which is deposited on GO surface. At the second stage, the thermal decomposition reaction of the intermediate product is conducted at 350 under the protection of nitrogen atmosphere, which is an intramolecular redox reaction because of the reducibility of $C_2O_4^{2-}$ and the oxidizability of Cu^{2+}. The redox reaction between $C_2O_4^{2-}$ and Cu^{2+} form Cu_2O phase and obtain Cu_2O/GO nanocomposites. The formation of the Cu_2O/GO nanocomposites is represented by the following chemical equations:

$$Cu_2(OH)_2CO_3(s) + H_2C_2O_4 \cdot 2H_2O(s) + GO \xrightarrow{ball\ milling}$$
$$Cu_2(OH)_{2n}(CO_3)_{1-n}C_2O_4/GO + (2-n)H_2O(l) + nCO_2(g)\ \ (1)$$

$$Cu_2(OH)_{2n}(CO_3)_{1-n}C_2O_4/GO \xrightarrow{calcined\ at\ 350°C\ under\ N_2}$$
$$Cu_2O/GO + nH_2O(g) + (3-n)CO_2(g)\ \ (2)$$
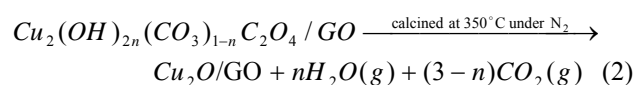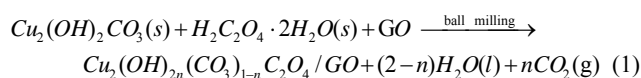
The XRD patterns of initial reactants and intermediate product obtained after 1h of milling are presented in Fig. 1. It can be seen from Fig. 1 that the diffraction peaks of the initial reactants completely disappear in intermediate product after 1h of milling, which indicate that the solid state reaction of $H_2C_2O_4 \cdot 2H_2O$ and $Cu_2(OH)_2CO_3$ is completed after 1h of milling.
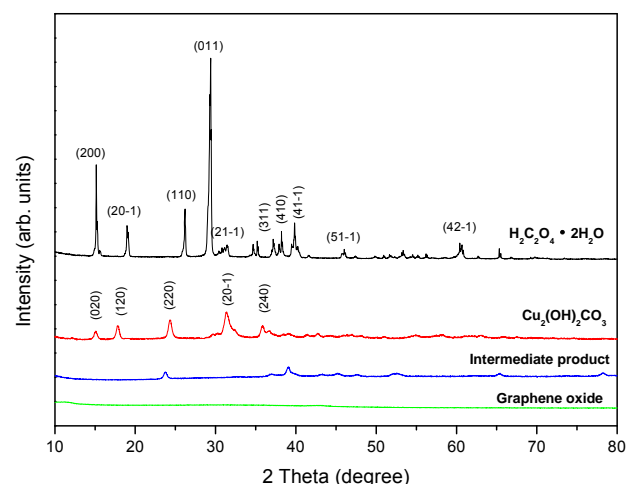
Fig.1. XRD patterns of reactants and intermediate product.

3.2 Influence of GO content on formation of Cu_2O/GO composites

The Cu_2O/GO composites with various GO weight percentages are synthesized by adjusting the GO amount added to the mixtures at a fixed mass of $Cu_2(OH)_2CO_3$. When the mass ratios of $Cu_2(OH)_2CO_3$ to GO are 5:1, 10:1, 20:1, 50:1, 70:1, the synthesized products are labeled as $5Cu_2O$/GO, $10Cu_2O$/GO, $20Cu_2O$/GO, $50Cu_2O$/GO and $70Cu_2O$/GO, respectively. Fig. 2 shows the X-ray

diffraction patterns of the Cu_2O/GO composites. From Fig. 2, the characteristic peak of cubic Cu_2O (JCPDS 65-3288) is observed in all samples and the intensity of Cu_2O diffraction peaks decreases gradually with the increase of the amount of GO. By calculating from Scherrer's equation, the crystallite sizes of Cu_2O in mCu_2O/GO composites are ca. 51, 51, 50, 50 and 49 nm corresponding to the m values of 70, 50, 20, 10 and 5, respectively. The results indicate that the crystallite sizes of Cu_2O in composites do not change or decrease only slightly with the increase of the amount of GO.
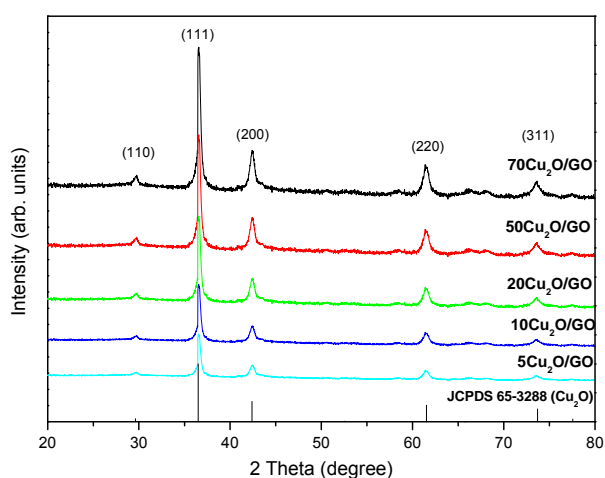
Fig.2. XRD patterns of the Cu_2O/GO composites with various GO weight percentages.

3.3 Morphology and microstructure of Cu_2O/GO composites

The morphology and microstructure of the Cu_2O/GO composites are characterized by TEM and SEM. Fig. 3 gives the typical TEM and SEM micrographs from $20Cu_2O/GO$. From Fig. 3, we can see that the as-synthesized Cu_2O crystals are cube-like particles, which are randomly distributed on the GO sheets due to the template effect of GO, consequently forming the Cu_2O/GO composites.
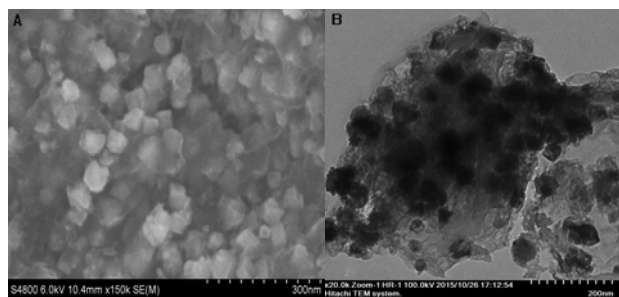
Fig.3. SEM and TEM images of the resultant $20Cu_2O/GO$ (A: SEM, B: TEM).

3.4 Photocatalytic activities of Cu_2O/GO composites

The photocatalytic activities of Cu_2O/GO composites with various GO weight percentages are evaluated by photocatalytic degradation of MO aqueous solution under visible-light irradiation, and experimental results are shown in Fig. 4. For comparison, the test result of the pure Cu_2O is also displayed in Fig. 4. It can be seen from Fig. 4 that mCu_2O/GO composites exhibit excellent photocatalytic activities in photocatalytic degradation of MO under visible-light irradiation and have higher photocatalytic activities than the pure Cu_2O. Moreover, it can be seen that the degradation percentage of MO follows the order of 89% ($50Cu_2O/GO$), 86% ($70Cu_2O/GO$), 81% ($20Cu_2O/GO$), 78% ($10Cu_2O/GO$), 75% ($5Cu_2O/GO$) after 60 min irradiation time. Although the photocatalytic activity of $50Cu_2O/GO$ is the best of all mCu_2O/GO composites, the activity of $5Cu_2O/GO$ is the highest in all composites according to the net content of Cu_2O.

The higher photocatalytic activities of the mCu_2O/GO composites compared to pure Cu_2O are ascribed to their excellent electronic conductivities and efficient separation abilities of photogenerated electron-hole pairs, large specific surface areas and high adsorption capacities. The detail photocatalytic degradation mechanism is demonstrated in Section 3.5.
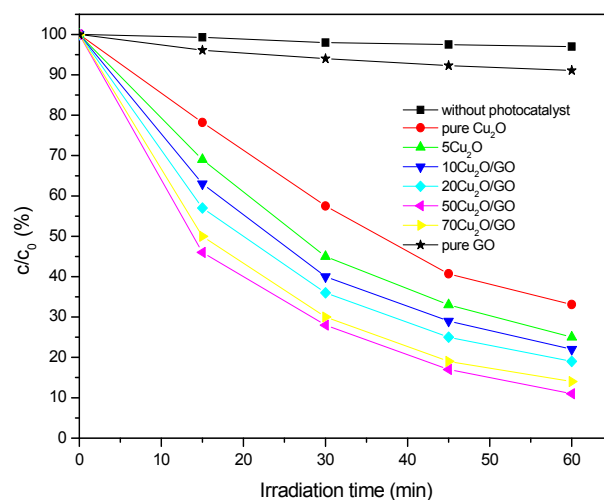
Fig.4. Photocatalytic activities of Cu_2O/GO composites.

3.5 Possible mechanism for enhanced photocatalytic performance of Cu_2O/GO composites

The graphene oxide has good capability to conduct and acts as an electron-transfer medium material. Thus, the graphene oxide in Cu_2O/GO composites plays a significant role in the efficient separation of photogenerated

electron-hole pairs and in promoting the photocatalytic redox reaction. So the Cu_2O/GO composites exhibit an enhanced photocatalytic activity than the pure Cu_2O for the photocatlytic degration of MO, which can be attributed to the synergistic effects of adsorption and photogenerated charge separation. Although the exact mechanism for the photocatalytic degradation of MO on Cu_2O/GO composites still needs further study, a possible photocatalytic mechanism can be proposed, as illustrated in Fig. 5.
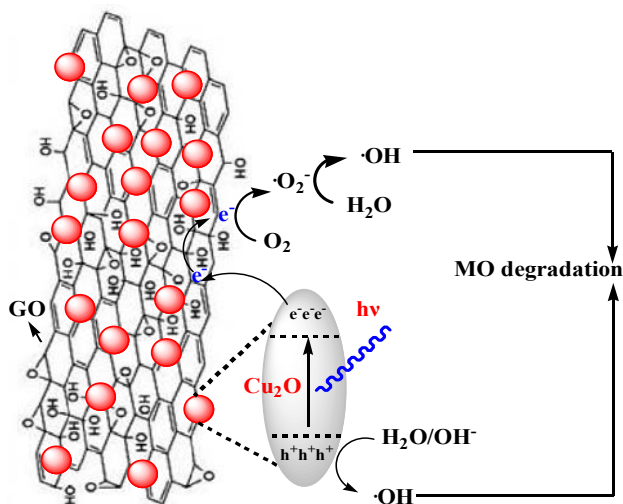
Fig. 5. Possible photocatalytic mechanism for MO over Cu_2O/GO composites.

According to the schema of Fig. 5, when the system is irradiated under visible light, Cu_2O is excited and the electrons (e^-) in the VB jump to the CB, with the same amount of holes (h^+) left in VB. Subsequently, the excited electrons can easily transfer from the CB of Cu_2O to GO. In such way, it is expect to achieve an efficient separation of the photoinduced electrons and holes, greatly reducing the recombination of the photogenerated charge carriers. Consequently, the enhanced photocatalytic activity of the mCu_2O/GO composites can be achieved. In the photocatalytic degradation of MO over mCu_2O/GO composites, Cu_2O in mCu_2O/GO composites is first excited under visible light and produce charge carriers. Then, the accumulated photoinduced electrons in the CB of Cu_2O can easily transfer to GO and they can be captured by O_2 adsorbed on the surface of GO to yield $\cdot O_2^-$, which is combined with H_2O to form $\cdot OH$. Meanwhile, the accumulated photoinduced holes in Cu_2O are also combined with H_2O or OH^- to form $\cdot OH$. Finally, those $\cdot OH$ will completely oxidize MO into to CO_2 and H_2O.

4. Conclusions

In this study, we have successfully synthesized the Cu_2O/GO nanocomposites by a simple one-pot method involving ball-milling assisted solid-state reaction and subsequent heat treatment. And this method also can be extended to other GO-based nanocomposites. The resultant Cu_2O/GO nanocomposites exhibit improved photocatalytic activities for the degradation of MO under visible-light irradiation compared to pure Cu_2O, indicating excellent photocatalytic performance and potential practical use. Experimental results also indicate that the amount of GO in the composites has very little effect on the crystallite sizes of Cu_2O in composites and has a certain influence on their photocatalytic activity. This study not only provides a new route to synthesize Cu_2O/GO nanocomposite photocatalysts, but also provides high efficient visible-light-driven photocatalysts for water purification and environmental remediation.

References

[1] L. F. Yang, D. Q. Chu, L. M. Wang, H. L. Sun, G. Ge, Mater Lett **159**, 172(2015).
[2] Z. Zhang, C. Zhong, L. Liu, X. W. Teng, Y. T. Wu, W. B. Hu, Sol Energ Mat Sol C **132**, 275(2015).
[3] X. H. Li, J. Q. Wang, Y. H. Zhang, M. H. Cao, Mater Res Bull **70**,728(2015).
[4] X. X. Zhang, J. M. Song, J. Jiao, X. F. Mei, Solid State Sci **12**,1215(2010).
[5] L. F. Li, W. X. Zhang, C. Feng, X. W. Luan, J. Jiang, M. L. Zhang, Mater Lett **107**,123(2013).
[6] L. Tang, Y. Du, C. Kong, S. Sun, Z. Yang, Phys Chem Chem Phys **17**, 29479(2015).
[7] Z. G. Niu, Mat Sci Semicon Proc **23**, 78(2014).
[8] X. Q. An, K. F. Li, J. W. Tang, Chem Sus Chem **7**, 1086(2014).
[9] P. D. Tran, S. K. Batabyal, S. S. Pramana, J. Barber, L. H. Wong, S. C. Loo, Nanoscale **4**, 3875(2012).
[10] A. Abulizi, G. H. Yang, J. J. Zhu, Ultrason Sonochem **21**,129(2014).
[11] F. G. Han, H. P Li, J. Yang, X. D. Cai, L. Fu, Physica E **77**,122(2016).

[12] Z. H. Zhang, S. Y. Zhai, M. H. Wang, H. F. Ji, L. H. He, C. M. Ye, C. B. Wang, S. M. Fang, H. Z. Zhang, J Alloy Compd **659**,101(2016).

[13] J. Miao, A. J. Xie, S. K. Li, F. Z. Huang, J. Cao, Y. H. Shen, Appl Surf Sci **360**, 594(2016).

[14] H. L. Xu, X. Q. Li, S. Z. Kang, L. X. Qin, G. D. Li, J. Mu, Int J Hydrogen Energ **39**, 11578(2014).

[15] Z. G. Niu, Mat Sci Semicon Proc **23**, 78(2014).

[16] M. Y. Wang, J. R. Huang, Z. W. Tong, W. H. Li, J. Chen, J Alloy Compd **568**,26(2013).

[17] Z. Y. Gao, J. L. Liu, F. Xu, D. P. Wu, Z. L. Wu, K. Jiang, Solid State Sci **14**, 276(2012).

[18] W. Z. Zou, L. Zhang, L. C. Liu, X. B. Wang, J. F. Sun, S. G. Wu, Y. Deng, C. J. Tang, F. Gao, L. Dong, Appl Catal B-Environ **181**, 495(2016).

[19] L. L. Sun, G. H. Wang, R. R. Hao, D. Y. Han, S. Cao, Appl Surf Sci **358**, 91(2015).

[20] A. L. Wang, X. S. Li, Y. B. Zhao, W. Wu, J. F. Chen, H. Meng, Powder Technol **261**, 42(2014).

*Corresponding authors: mlzhang1268@163.com
once1970@sina.com